Hypothesis Testing Detection of Mines Buried Under Rough Ground *Surfaces using 2-D FDTD Modeling

He (Sophia) Zhan[*a], Carey Rappaport[**a], Magda El-Shenawee[b], Eric Miller[a]

[a] Center for Subsurface Sensing and Imaging Systems
Department of Electrical and Computer Engineering
Northeastern University, 235 Forsyth Building, Boston, MA 02115

[b] Department of Electrical Engineering, 3217 Bell Engineering Center,
University of Arkansas, Fayetteville, Arkansas 72701

ABSTRACT

In ground penetrating radar (GPR) antipersonnel mine sensing, in which the target is small, shallow and often of low dielectric contrast, detection is challenging. One of the difficulties is that it is hard to distinguish the target signal from the omnipresent random rough ground reflection clutter. In this work, a Monte Carlo computational simulation using 2-dimensional (2-D) transverse magnetic (TM) finite difference time domain (FDTD) with multiple rough surfaces is implemented to investigate single TNT target buries in dispersive soil.

Based on the effects of the random rough surface on an impulse GPR signal and the knowledge of wave propagation differences in different media – air, soil, and TNT – a special background average process using physics based signal processing (PBSP) is performed to remove the ground clutter signal. This procedure first involves shifting and scaling multiple time signals from target-free random rough ground to establish the nominal (average) ground reflection pulse shape. Next, this nominal pulse shape is correlated in time with each trial signal, then shifted and scaled to match the ground surface clutter of that trial signal. Subtracting this shifted scaled clutter signal from the trial signal ideally leaves the target signal (with some additional multiple scattering between the target and ground surface). The PBSP algorithm reapplied in cases for which surface scattering occurs at multiple points. The statistical results of PBSP surface clutter removal indicate that the detection performance degrades with increasing surface roughness and decreasing burial depth. Hypothesis testing on the processed results proved to be successful in a detection and estimation point of view. This paper presents the detection performances in terms of Receiver Operating Characteristics (ROC) for various ground surface roughness and target burial depth cases. Also demonstrated is the performance improvements expected from multiple views: indicating that a multi-bistatic configuration appears to be superior to multistatic transmitter/receiver geometry with minimum combinations.

Keywords: hypothesis testing, FDTD, GPR, ROC, performance, bistatic

1. INTRODUCTION

Detecting buried dielectric targets – such as antipersonnel mines – with GPR is important since million of mines are still be hidden in the ground, a cost and labor effective technique is needed. However, it is also challenging, because the dielectric constant of nonmetallic mine targets are similar to those of the surrounding soil, and because their sizes are comparable to the thickness of soil layer above them. In addition, the soil dielectric constant may not be well characterized, and the ground surface will usually be rough, often with roughness of the order of the target burial depth. The focuses of mine detection addressed in this paper are ground clutter removal and hypothesis testing which qualifies

*hzhan@ece.neu.edu; phone (617)373-4874; 467 Egan Research Building, 320 Huntington Avenue, Boston, MA 02115
**rappaport@neu.edu; phone (617)373-2043; fax: (617)-373-8627; 302 Stearns Center, 320 Huntington Avenue, Boston, MA 02115

Detection and Remediation Technologies for Mines and Minelike Targets VII, J. Thomas Broach, Russell S. Harmon, Gerald J. Dobeck, Editors, Proceedings of SPIE Vol. 4742 (2002) © 2002 SPIE · 0277-786X/02/$15.00

the detection performance based on 2D TM FDTD model. Although 3D FDTD is more accurate and visible, it is computationally complex and expensive while 2D FDTD can provide much information.

The computational geometry shown in Fig. (1) is typical bistatic geometry based on the Geo-Centers, Inc. EFGPR system[1]. The measured Geo-Centers TEMR GPR antenna element radiated signal is used as the excitation, shown in Fig. (2). The TEMR is a wide-band antenna, throughout the 200MHz to 2.0GHz range.

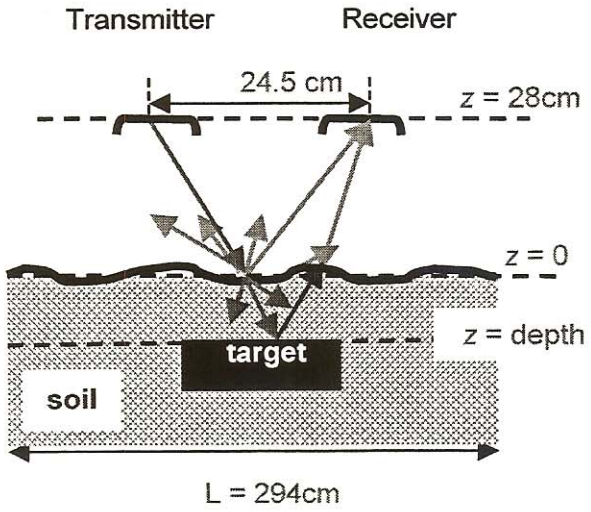

Figure 1. Rough surface computational geometry

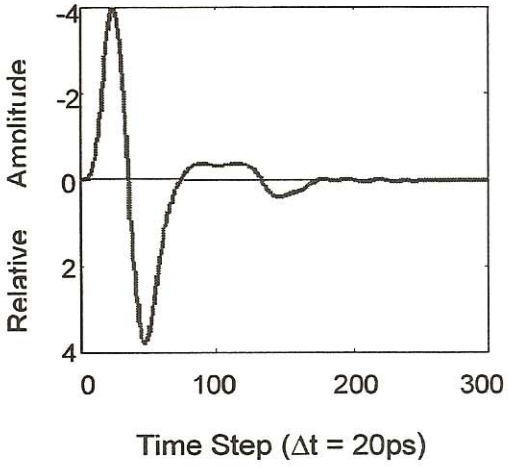

Figure 2. incident measured waveform

The impulsive electromagnetic wave propagates through the dispersiver soil and is partially reflected. The received components in time are: the transmitter-receiver coupling signal with much stronger amplitude than the target signal; the ground reflection clutter signal, with distorted shape due to surface roughness; and the target return that is buried in the clutter.

The soil model is Puerto Rican clay loam[2] with 10% moisture and 1.4g/cc density, with average dielectric constant $\varepsilon' = 6.2$. Since the soil is frequency-dependent medium, it is modeled by a single pole conductivity model based on the observation that the frequency variation of the real dielectric constant does not significantly affect either the real propagation constant or the decay rate[3,4,5]. The probability density function for the random height of the ground surface has a Gaussian distribution with zero mean and standard deviation σ_h. Also, the surface profiles spectrum is assumed Gaussian[6,7]. Since we interest in the clutter effects on target discrimination, the single scale Gaussian assumption is reasonable[8].The frequency-independent target is the dry TNT with dielectric constant 2.9, and almost 0 conductivity[9], and its size is about 10cm by 5cm.

In the FDTD[10] code, the time step used was Δt = 20ps, which is matched to the 2D excitation time interval, and spatial difference is calculated to be Δ = 1.22cm. The boundary condition used is the perfect matched layer (PML) absorbing boundary condition[11], with which the theoretical reflection factor of a plane wave striking a vacuum layer interface can be made insignificant at any frequency and at any incidence angle. In this computation, 16 PML half-layers are used, and it gives good result for incident angle less than 75 degrees[12].

The simulations are implemented for a variety of rough surfaces characterized by standard deviation for height σ_h and correlation length l_c, also for various depths of buried target, and without target as well. In each simulation, 500 random rough surface realizations are generated.

2. SIGNAL AND CLUTTER SEPARATION MODELING AND PROCESSING

The goal of the process is to maximally suppress the clutter and retain the target signature. Since the surface is rough, the statistical rough ground reflection signal is obtained by the cross-correlation model, and eliminated from the received signal. Furthermore, because the shift of target signal is related to the shift of the ground clutter signal, the target signal is enhanced by the alignment procedure.

When the correlation length l_c is large, the received pulse is a shifted and scaled version of transmitted signal. The time shifting and amplitude scaling are due to air/soil partition of the wave propagation path. By identifying these parameters and measuring their statistics separately, much added information about the ground clutter becomes available. The time shifting is found by the correlation function. Cross-correlation function between reference signal 'f', which is from an ideal soil half-space with a flat boundary, and any realization signal 'i' is[7,13]:

$$C_{fi}(m) = \sum_{n=1}^{N-|m|} S_f(n) S_i(n+m) \Big/ \sqrt{\sum_{n=1}^{N} |S_f(n)|^2} \sqrt{\sum_{n=1}^{N} |S_i(n)|^2} \qquad for \quad m \geq 0 \tag{1}$$

$$C_{fi}(m) = C_{if}(-m) \qquad for \quad m \leq 0 \tag{2}$$

The relative scaling is obtained from:

$$A_i = \sqrt{\sum_{n=1}^{N} |S_i(n)|^2} \Big/ \sqrt{\sum_{n=1}^{N} |S_f(n)|^2} \tag{3}$$

where $i = 1,2,\ldots M$ is the rough surface realization index, M is the size of Monte Carlo sample, and N is the total number of time steps. Another way to obtain the scaling factor is to use the maximum correlation normalization instead. Since the energy normalization is superior for rougher surfaces that generate greater pulse distortion, the relative scaling is calculated using Eq. (3). The flow chart of the PBSP is shown in Fig.(3).

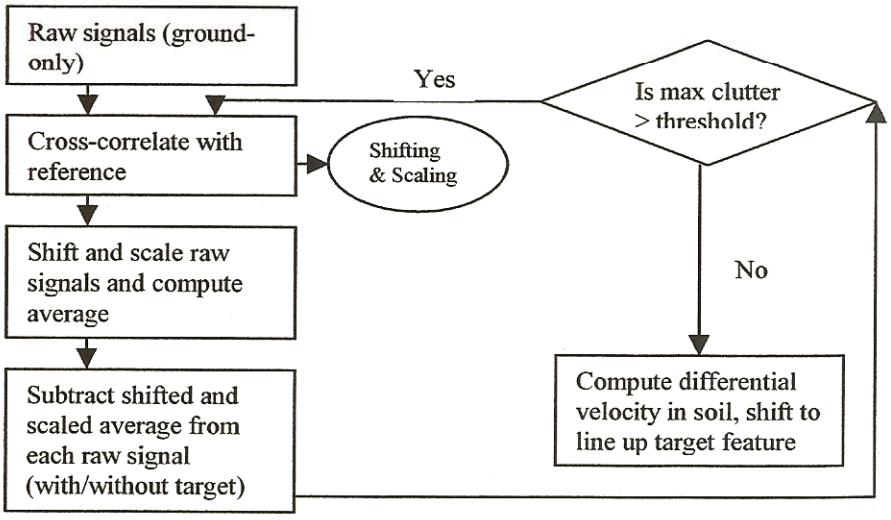

Figure 3. Flowchart of single/multiple PBSP to suppress the ground clutter(s)

The nominal background signal is found by shifting received ground-only signal by $\tau_{gnd,i}$, scaling by A_i, and averaging. The ensemble average gives the best estimate for the local clutter that corrupts the target signal. To reduce ground clutter, the nominal background signal is then shifted back by $\tau_{gnd,i}$, scaled by A_i, and subtracted from each received signal S_i. With the assumption or the knowledge of the depth of the buried target, the path of the scatter signal can be estimated. The wave propagation velocity in soil compared with that of in air is reduced by a factor $1/\sqrt{\varepsilon}$, the shifting factor for the target signal $\tau_{\min e,i}$ due to the change of soil amount can be calculated according to the geometry path. Then, the background-subtracted signals are once again realigned to the expected target position[7,13]. If the surface scattered wave were primarily due to a single specular reflection – as would be the case if l_c were large – then this procedure would suppress most of the surface clutter. However, it is possible that the surface scattering occurs at multiple points. In that case, the cross-correlation/shifts ensemble average/subtraction procedure is repeated.

One hundred computed scattered signals with/without in-ground-target are shown in Fig. (4.a1) and Fig. (4.b1) along with the ±1 standard deviation confidence interval, with the direct transmitter-receiver coupling signals removed. Those two plots are almost identical. Then, the ground clutter removal procedure is applied, with results shown in Fig. (4.a2) and Fig. (4.b2). Comparing the target-free mean plot to the target-in-ground mean plot, although there are clutter variations involved, there is visible difference in time interval [200 300] – where the target signal would be expected to occur. Therefore, it is possible to distinguish target-in-ground plot from target-free plot. However, it is difficult to localize the target to a certain depth by only looking at Fig. (4.b2), since the clutter amplitudes are comparable to those of the target signal. The realigned signals of the complete PBSP procedure are plotted in Fig. (4.a3) and Fig. (4.b3). The target signals are now well aligned, and the target position can be located by investigating the mean signal in the target-in-ground plot. Furthermore, as expected, the standard deviation is much smaller for the target region of the signal than for the clutter region. The double clutter removal results are shown in Fig. (4.a4) and Fig. (4.b4). Since the clutter due to the second ground reflection has been suppressed, the amplitude of the clutter signal is reduced. Meanwhile, the target signature remains as prominent as expected.

By using the PBSP, most of the ground clutter can be suppressed. However, the processing results are roughness dependent and related to the depth of a buried target. In Fig. (5), the mean signal and STD of several rough surfaces and various depth cases are present.

3. SIMPLE BINARY HYPOTHESIS TESTING

We simplify the mine detection problem to be: whether there is mine at certain depth with the knowledge of the surface roughness. Each of the two answers corresponds to a hypothesis:

H_1 corresponds to the presence of a target (i.e., mine is present)
H_0 corresponds to the absence of a target (i.e., no mine)

Applying the likelihood ratio test, which is derived to be[14]:

$$-\frac{1}{2}\left(\mathbf{r}^T-\mathbf{m}_0^T\right)\mathbf{Q}_0\left(\mathbf{r}-\mathbf{m}_0\right)-\frac{1}{2}\left(\mathbf{r}^T-\mathbf{m}_1^T\right)\mathbf{Q}_1\left(\mathbf{r}-\mathbf{m}_1\right)\underset{H_0}{\overset{H_1}{\gtrless}} threshold \tag{4}$$

where $\mathbf{r}$, $\boldsymbol{m}_0$ and $\boldsymbol{m}_1$ are vectors with N elements, $\boldsymbol{Q}_0$ and $\boldsymbol{Q}_1$ are N x N covariance matrices. $\mathbf{r}$ represents the individual background-subtracted signals. $\boldsymbol{m}_0$ is the average of realigned no target (clutter) signals; $\boldsymbol{m}_1$ is the realigned target signals. The covariance matrices $\boldsymbol{Q}_0$ and $\boldsymbol{Q}_1$ are the inverses of the diagonal matrices of standard deviations of the clutter and target signals. Since the processed signals are not guaranteed independent of one and another, the diagonal covariance matrices used in the test are approximations. We are investigating the worse case hypothesis test here. 100 out of 500 target signals and 100 out of 500 clutter signals are grouped at test signals. The average signals $\boldsymbol{m}_0$ and $\boldsymbol{m}_1$, and standard deviations are obtained form the remaining 400 clutter signals and 400 target signals. The likelihood ratio

test is applied to each test signal associated with a set of trial thresholds. Subsequently, the probability of *false alarm* P_F (*i.e.*, we say the target is present at certain depth when it is not) and the probability of, detection P_D (*i.e.*, we say the target is present at certain depth when it is) are obtained. The performance of the likelihood ratio test is evaluated by receiver operating characteristic (ROC) curve[14]. The ROC curves for a variety of rough surfaces and different depths are shown in Fig. (6). As the depth increases, the performance improves, *i.e.*, when a buried target is close to the surface, it is hard to distinguish the ground clutter from the target signal since the ground clutter signal and target signal are too close to remove the clutter signal without affecting the target signal. The detection performance degrades as the standard deviation increases. Thus, the detection becomes difficult as expected when the surface is rough and the target is shallow buried.

By relating signals associated with certain depth to several average signals for different depths, it has been found that the best performance always occurs for the correct depth estimate. An example is shown in Fig. (7). The test signals for depth 8.5cm were related to the average signals and corresponding standard deviation that are belong to the same roughness family. Thus, the correct target depth will be obtained by testing sample signals with stored statistics of various families with same surface roughness. Interestingly, the ROC curves for close but not exact depths are worse than those for much deeper or shallower depth estimates.

The previous results are based on the geometry shown in Fig. (1) -- the target is centered beneath the transmitter-receiver (TR) pair. Recall that the detection performances decrease for rougher surfaces. In order to improve the performance, multi-bistatic and multistatic geometries are investigated. Now, in addition to then single centered TR pair position, we used four more TR positions for multi-bistatic geometry: 12.2cm and 24.4cm to the left and right of the center. As the pair moves away from the target, the test performance degrades. Also, the amplitude of the average target signal drops. However, the combination of three TR positions improves the detection performance significantly. With five TR views, the performance is even better. It is also true for the multistatic case with fixed transmitter and multiple receiver views. The improvements of using three/five TR pairs and three/five receiver views are shown in Fig. (8.a) and Fig. (8.b). Although performance increases with the number of views, the combinations of three TR positions, or three receiver views, each spaced 12.2cm apart to the left and right, appear to give excellent results.

4. CONCLUSIOIN

The computational study of 2D TM FDTD is presented to investigate a single dry TNT target at certain depth buried in dispersive soil with the presence of a random rough surface. The dispersive FDTD algorithm is used to incorporate the frequency-dependent complex conductivity media – Puerto Rican clay loam. The air/soil interface is characterized by Gaussian roughness, since the single scale roughness is well described by Gaussian process. The GPR impulse used is based on a measured transmitter pulse, with a wide-band width and the capability of exploring target in the presence of a lossy medium. The PML boundary is employed to terminate the computational grid.

The simulated result is processed using a background average procedure – PBSP, which even works for a shallow buried target. The ground clutter is mostly removed by the ensemble average and subtraction procedure. Also, shifting and scaling the individual received signal back and forth according to the transmission path in the air and the soil enhance the target signature. The statistical results of the PBSP indicate that the quality of target signals depends on the roughness of the surface and the depth of a buried target.

In addition to examining the statistics of fields scattered from a Gaussian rough surface, we investigate the worse case target detection performance by using the classic detection theory. Applying the binary hypothesis tests to the processed signals, the target can be localized at certain depths even under rough ground surfaces. Furthermore, the spatial combinations of TR position will improve the detection performance.

ACKNOWLEDGEMENT

This work is supported by the Army Research Office ground No. DAAG55-97-0013.

REFERENCES

1. C. Rappaport and D. Reidy, "Focused array radar for real time imaging and detection', in Proc. Of SPIE, vol. 2747, pp.202-213, (Orlando, FL), Apr. 1996
2. J. Hipp, "Soil Electromagnetic Parameters as Functions of Frequency, soil Density and Soil Moisture," *Proceedings of the IEEE,* vol. 62, no, 1, Jan.1974, pp. 98-103
3. C. Rappaport, S. Wu, and S. Winton, "FDTD wave propagation in Dispersive soil using a single pole conductivity model", accepted for publication in *IEEE Trans. On Magnetics,* May 1999
4. W. Weedon, and C. Rappaport, "A General Method for FDTD Modeling of Wave Propagation in Arbitarty Frequency-Dispersive Media", *IEEE Transaction of antennas and Propagation,* pp. 401-410, March 1997
5. C. Rappaport and S. Winton, " Modeling Dispersive soil for FDTD Computation by Fitting Conductivity Parameters", *12th Annual Review of Progress in Applied Computational Electromagnetics Symposium Digest,* pp. 112-118, March 1997
6. P. Beckmann and A. Spizzichino, *The Scattering of electromagnetic Waves from rough surfaces,* New York, 1963
7. M.El-Shenawee, C. Rappaport, " Quantifying the Effects of Different Rough Surface Statistics for Mine Detection Using the FDTD Technique", *Proc. SPIE,* April 2000
8. E.I.Thorson, "The validity of the Kirchoff approximation for rough surface scattering using a Gaussian roughness spectrum", *J. Acoust. Soc. Amer.,* vol. 83, pp.78-92, 1988
9. A. von Hippel, *Dielectric Materials and Applications,* Wiley, New York, 1953
10. K. Yee, "Numerical solution of initial boundary value problems involving Maxwell's equations in isotropic media", *IEEE Trans. Antennas Propagat.*, vol. AP-14, pp302-307, May 1966
11. J. Berennger, "A Perfectly Matched Layer for the Absorption of Electromagnetic Waves", *Jour. of Comp. Phys.*, vol. 114, pp 185-200, Oct. 1994
12. C. Rappaport, M. Kilmer and E. Miller, " Accuracy considerations in using the PML ABC with FDTD Helmholtz equation computation", *International Jounal of Numerical Modelling: Electronic Networksm Devices and Fields"* vol.13, pp.471-482, 1999
13. C.Rappaport, M.El-Shenawee, " Modeling GPR Signal degradation from random rough Ground surface ", *IGARSS,* Honolulu, HI, July 2000
14. H. Van Trees, "Detection, Estimation, and Modulation Theory", John Wiley and Sons Inc., 1968

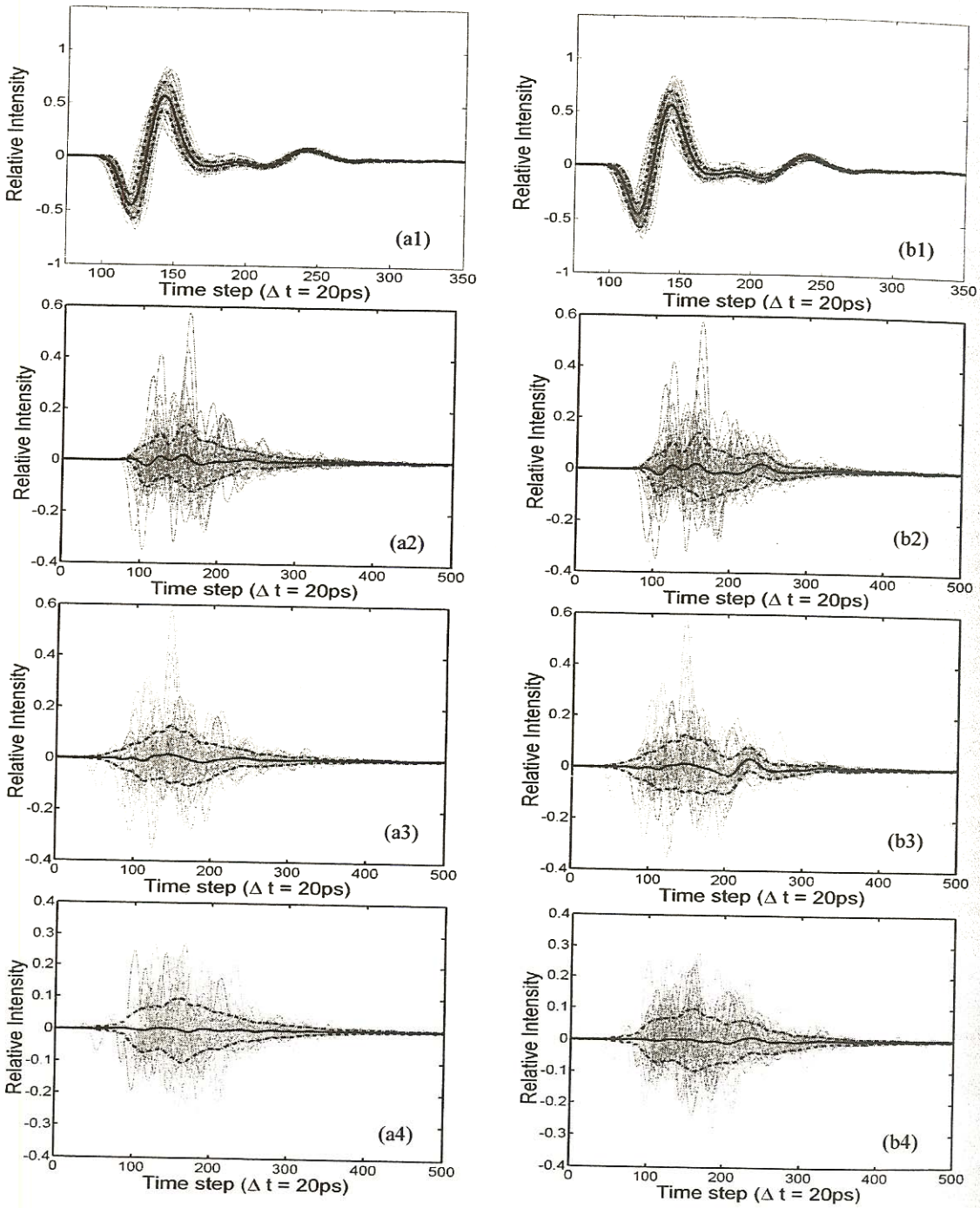

Figure 4. For case $(\sigma_h = 3, l_c = 10, z = 8.5)cm$

(a1) target-free raw signals; (b1) target-in-ground raw signals
(a2) ground clutter removed target-free signals; (b2) ground clutter removed target-in-ground signals
(a3) realigned target-free signals; (b3) realigned target-in-ground signals
(a4) double-clutter removed and realigned target-free signals; (b4) double-clutter removed and realigned target-in-ground signal

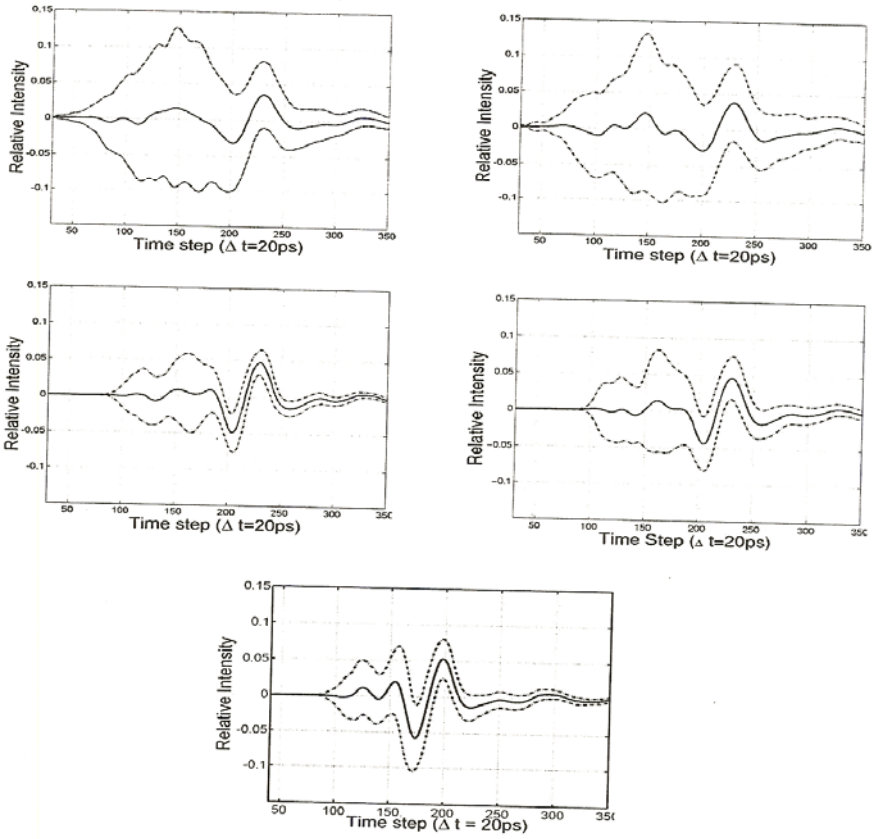

Figure 5. Mean signal and STD for several rough surfaces and various depths.
(a) $(\sigma_h = 3, l_c = 10, z = 8.5)cm$: (b) $(\sigma_h = 3, l_c = 3, z = 8.5)cm$
(c) $(\sigma_h = 1, l_c = 10, z = 8.5)cm$: (d) $(\sigma_h = 1, l_c = 3, z = 8.5)cm$
(e) $(\sigma_h = 1, l_c = 10, z = 4.8)cm$

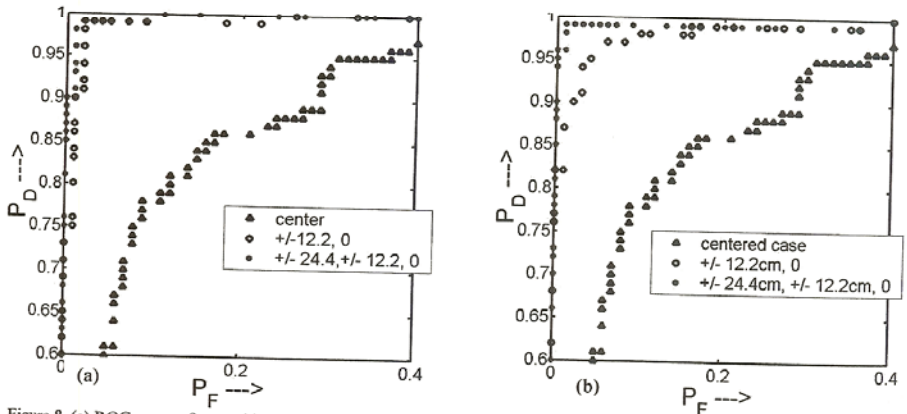

Figure 8. (a) ROC curves for combinations of 1,3,5 TR pairs; (b) ROC curves for combinations for 1,3,5 R views.